Polyamide 6 recycled fishing nets modified with biochar fillers: An effort toward sustainability and circularity

Materials Today Communications 41 (2024) 110650

Contents lists available at ScienceDirect

Materials Today Communications

journal homepage: www.elsevier.com/locate/mtcomm

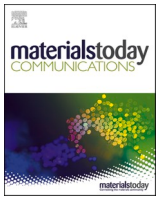

Polyamide 6 recycled fishing nets modified with biochar fillers: An effort toward sustainability and circularity

Damiano Rossi [a,*], Miriam Cappello [a], Sara Filippi [a], Mattia Bartoli [b], Giulio Malucelli [c], Patrizia Cinelli [a], Maurizia Seggiani [a]

[a] Department of Civil and Industrial Engineering (DICI), University of Pisa, 56122, Italy
[b] Center for Sustainable Future Technologies - CSFT@POLITO, Torino, 10144, Italy
[c] Department of Applied Science and Technology (DISAT), Politecnico di Torino, 10129, Italy

ARTICLE INFO

Keywords:
Polyamide 6
Rice husk biochar
Lignocellulosic biochar
Mechanical behaviour
Sustainability

ABSTRACT

In a further research effort toward sustainability and circularity, this work demonstrates the possibility of designing and producing novel blends derived from recycled polyamide 6 (PA6) fishing net, incorporating two biochars, i.e., carbonaceous materials obtained from the controlled pyrolysis of vegetable biomasses, at different loadings (namely 5, 10, and 15 wt%). The biochar derived from lignocellulosic biomass enhanced both the mechanical properties and moisture resistance of the recycled polyamide, increasing the elastic modulus from 2.6 to 4.5 GPa and reducing water uptake from 3.6 % to 1.8 %. Interestingly, thanks to its high silica content, the biochar derived from rice husk accounted for an increase in the activation energy for combustion of the polymer matrix (from 43.6 to 70.9 kJ/mol). However, it also showed a detrimental effect on the water uptake and the mechanical behaviour of the blends. Besides, the possibility of replacing up to 15 wt% of petroleum-derived carbon black pigments with the biochars decreased the overall cost of PA6 blends. Also considering the biochar densities that are lower than those of traditional carbon fillers, the proposed blends may pave the way for the design, development, and exploitation of novel sustainable materials suitable for lightweight applications.

1. Introduction

Plastics are widespread in our society due to their exceptional properties and cost-effectiveness, making them indispensable across various sectors, notably within the packaging and construction industries (~ 60 % of the overall plastic production). Recent data indicate a demand for around 57.2 million tons of plastics in Europe in 2022 [1], with production rates increasing rapidly. This trend poses significant challenges to global ecosystems, especially marine habitats [2–4]. It is estimated that around 11 million tons of plastic debris are improperly disposed of in the oceans annually, with a projected trend that could nearly triple by 2040 [5]. In this scenario, governments and industries are implementing measures to reduce plastic debris stemming from land-based activities. Nevertheless, the challenge persists in managing plastic wastes generated by marine activities, such as fishing. Around 20 % of the overall plastic accumulation in oceans (about 640,000 tons per year) is attributed to fishing nets, and fishing accessories [6,7]. Following the 2020 PETI Report of the Council of the European Union, significant resources will be allocated for the development of innovative methods aimed at reusing and recycling these products within a circular economy framework [8]. However, there is currently no dedicated recovery system for plastic materials from marine activities, highlighting the critical need for effective recycling strategies to address this type of plastic pollution.

Recycling fishing products presents hurdles due to the complexities of material collection, sorting, and re-processing. Fishing gears are typically fabricated from a variety of robust, resilient, and durable polymers, including nylon 6 (polyamide 6, PA6), nylon 66 (polyamide 66, PA66), high-density polyethylene (HDPE), ultra-high molecular weight polyethylene (UHMWPE), and polypropylene (PP). These materials are not biodegradable and require significant resources and energy demand for their mechanical sorting and thermal recycling via melt compounding [9]. Another issue to be addressed is the presence of organic residues and sea salt, which requires a thorough cleaning phase that consequently raises the costs associated with the recycling processes [10]. To improve cost-effectiveness and properties, as well as to

* Corresponding author.
E-mail address: damiano.rossi@unipi.it (D. Rossi).

https://doi.org/10.1016/j.mtcomm.2024.110650
Received 20 August 2024; Received in revised form 2 October 2024; Accepted 7 October 2024
Available online 9 October 2024

broaden the utilization of recycled fishing nets as raw material, blending them with virgin resins at different percentages may ensure suitability for the envisaged applications. In fact, the combination of virgin and recycled materials has emerged as a viable strategy for the reuse of these plastic materials as we move toward a circular marine plastic economy [11].

The recycling rates of fishing nets vary depending on their ease of recyclability and accessibility. PA6 and PA66 nets are widely used, especially in the production of gill nets, owing to their exceptional durability and flexibility. Currently, polyamide nets undergo mechanical recycling and, to a lesser extent, chemical recycling through depolymerization [12,13]. Conversely, fishing nets made of HDPE and PP hold less economic value since both are commonly employed for the manufacturing of trawl nets, which are prone to abrasive damage and thus are more difficult to recycle into new products. The market for products derived from recycled fishing nets includes fabrics, clothing, and small accessories commercialized by Patagonia NetPlus® and PlastixGlobal® [14–16]. Furthermore, recycled fishing plastics are employed in the construction and building sector as reinforcement in cementitious materials [17]. The automotive industry is another emerging sector, where thermoplastic fibres and fillers are gradually introduced to develop new lightweight materials and composites. Recently, the EU introduced updates to the End-of-Life Vehicles (ELV) Regulation to promote the circularity of vehicles and set ambitious recycling targets to ensure that at least 25 % of plastics used in vehicle construction derive from recycled materials. In line with this initiative, next-generation Jaguar and Land Rover models will incorporate floor mats and trims crafted from Econyl® fibre, derived from recycled nylon possibly recovered from fishing nets. Additionally, LyondellBasell launched Circulen-Recover®, a new injection-moulded recycled PP copolymer tailored for automotive applications, produced from recovered maritime plastics [18,19].

Additives like plasticizers, stabilizers, and fibres are typically used in combination with recycled plastics to mitigate the loss of physical properties due to mechanical and thermal re-processing. Moreover, the integration of low-cost renewable additives enhances material affordability and sustainability. Among these sustainable additives, biochar stands out as the solid residue obtained from thermal cracking (500–900 °C) of biomass in an oxygen-poor atmosphere. While biochar has typically been used for water pollutant remediation and soil amendment [20], emerging applications include its adoption as a more sustainable substitute to conventional fillers such as carbon black in polymer composites, thanks to its high compatibility and thermal/electrical conductivity [21–25]. Biochar porous structure results in biocarbon composites with lower density than traditional talc and carbonate-based counterparts, making it a suitable filler for developing lightweight materials, especially in combination with polyamides [26,27]. In polymer systems, the inclusion of biochar significantly improves both mechanical strength and stiffness, while reducing impact toughness and ductility [24,28–32]. Furthermore, the addition of biochar limits the water uptake and the consequent hydrothermal ageing processes [27,28]. Interestingly, biochar also exhibits thermal stability and flame-retardant properties [28,32,33] and has the potential to substitute more traditional flame-retardants such as ammonium polyphosphate and magnesium hydroxide [34,35].

Polymers with good flame-retardant properties help limit the fire spread and reduce the risk of fires in critical situations. Based on UN-ECE R118 and ISO 3795 regulations, these properties are crucial in road vehicle construction, particularly for interior components, panels, cables, and other materials that might be exposed to irradiative heat sources or direct flames during a fire occasion. Recently, various carbonaceous fillers, such as graphite [36], clays [37], and carbon nanotubes [38], have been explored as alternatives to traditional chemical flame-retardants to alleviate their adverse environmental effects. Among these, biochar obtained from silica-rich rice husk accounts for a unique combination of sustainability, biodegradability, and cost-effectiveness. The flame-retardant properties of polymer composites filled with silica-rich components were attributed to the thermal shielding effect provided by the ceramic filler layer that originates during the combustion [39]. The use of rice husk has been investigated not only with such polyolefins as LDPE, HDPE [28,32,40,41], and PP [42,43], but also with biobased polymers like PLA [33,44–46] to improve water resistance, particularly in coatings. Interestingly, Zhang et al. developed high-loaded PE-based composites incorporating rice husk, achieving a limited oxygen index of around 25 %, indicating potential flame-retardant properties [32]. Recently, Hoang et al. demonstrated the efficacy of rice husk in inhibiting heat transfer and mitigating thermal degradation during the combustion of polypropylene [28].

In this context, the current study investigates the potential for creating new sustainable blends derived from discarded PA6 fishing nets, aiming to improve their thermal, rheological, and mechanical properties through the incorporation of biochar fillers. This represents the main novelty of the proposed investigation, which refers to the possibility of revalorizing PA6 material at the end of its life by designing polymer-biochar blends with improved characteristics. Besides, this strategy accounts for a high circularity, hence becoming very important to the revalorization of a waste, the quantity of which is substantial and deserves to be repurposed.

The use of the two biochars, i.e., a traditional lignocellulosic biochar and a silica-rich biochar produced from rice husk, in recycled PA6 nets was assessed by fabricating pellets via melt extrusion at different filler loadings (namely 5, 10, and 15 wt%). The resulting blends were characterized through Fourier Transform Infrared spectroscopy (FT-IR), Raman spectroscopy and electron microscopy (FE-SEM) to assess the molecular interactions occurring between the PA6 matrix and the filler. Additionally, Differential Scanning Calorimetry (DSC) and Thermogravimetric Analysis (TGA) were employed to study the thermal behaviour of the PA6/biochar blends. Constant heating rate thermogravimetric analysis was exploited to study the thermal degradation kinetics with the method developed by Flynn, Wall, and Ozawa [47,48]. Furthermore, water uptake and rheological behaviour of the blends were examined to assess the influence of biochar on moisture absorption and processability, respectively. Finally, the mechanical properties were determined through tensile tests conducted on dog-bone specimens.

2. Experimental

2.1. Materials

Monofilament polyamide 6 (P) fishing nets were collected from the nearby port of Livorno, and washed to remove sand, sea salt, and organic residues. Lignocellulosic biochar (B) of class I quality, derived from the pyro-gasification of vegetable biomass, was supplied by BioDea Srl (Arezzo, Italy). This biochar filler contains 3–5 wt% of ash, 67–75 wt% of C, 0.2–0.4 wt% of total N, 0.03–0.04 wt% P, and traces of elements such as Fe, Na, K, Ca, and Mg. Rice husk biochar (RH) was produced from rice husk initially stabilized in a ventilated oven at 105 °C for 72 h. Then, the husk were subjected to pyrolysis in a tubular oven set at 550 °C, in inert atmosphere (N_2), with a heating rate of 10 °C/min, and maintained at the maximum temperature for 30 min. Both biochars present similar particle size distributions in the 5–100 μm range.

2.2. Blends preparation

B and RH biochar powders were first dried at 110 °C for 48 h to remove moisture. The P nets were also dried overnight in a vacuum oven at 100 °C and pelletised using a granulator Shini SG-3048 by Chinchio Sergio Srl (Brescia, Italy). The blade-to-blade distance was fixed to produce small cylindrical cuts measuring 0.5–1 mm in diameter and 2–4 mm in length. Then, mixtures of P/B and P/RH with different biochar content (5, 10, and 15 wt%) were processed using a single-screw extruder by Brabender GmbH (Duisburg, Germany). These blends are

identified as PBX and PRHX, where X represents the biochar wt% loading. The various blends were produced using a consistent feed-to-head zone temperature profile of 50 | 180–200 | 240–245 | 250–255 | 240–245 °C. During processing, the screw remained steady at 30–35 rpm, with a mean torque value ranging from 12 to 18 Nm and a mass rate of about 2 kg/h. An increase in biochar content beyond 15 wt % resulted in significantly elevated torque and extreme thermal conditions, possibly causing excessive stresses and degradation of the polymer matrix. To evaluate the effect of melt processing on the thermal and mechanical properties, the virgin P net was also processed under the same conditions (P' denotes the P net post-processing). After extrusion, the filaments were cooled in a water bath at room temperature, and then automatically cut into pellets using a Procut 3D by Chinchio Sergio Srl (Brescia, Italy) cutter. These pellets were finally dried at 100 °C for 24 h in a vacuum oven and sealed in vacuum bags to prevent moisture absorption before conducting the different characterization analyses.

2.3. Characterization methods

2.3.1. Fourier transform infrared spectroscopy (FT-IR) and raman spectroscopy

FT-IR spectra were acquired to explore potential molecular interactions between the functional groups of nylon 6 and those present in biochar. The spectra were recorded in ATR mode using a spectrometer Cary 630 FT-IR by Agilent Inc (CA, US) over the wavenumber range from 4000 to 400 cm^{-1} with a scanning resolution of 4 cm^{-1}. Before analysis, all pellets (P, P', PBX, and PRHX) were pre-dried at 40 °C in a vacuum oven for approximately 24 h.

Raman spectra were collected using an inVia Apparatus H43662 by Renishaw plc (Gloucestershire, UK) equipped with a laser line (wavelength of 532 nm) in the range from 500 to 3500 cm^{-1}. The deconvolution of signals was performed with a Matlab (version R2020a) homemade compiled software according to Tagliaferro et al. [49].

2.3.2. Thermal analysis

Differential Scanning Calorimetry (DSC) was performed on the different pellets to assess the influence of biochar addition on the crystallinity of the blends. The analysis was carried out using a DSC Pyris 1 6000 by Perkin Elmer Inc (Waltham, USA) with a nitrogen flow of 50 ml/min. Approximately 20 mg of each sample was placed in a hermetically sealed aluminum pan and heated at 10 °C/min from −40 °C to 330 °C to eliminate any thermal history from processing. The sample was held at 250 °C for 3 min, then cooled down to −50 °C at 10 °C/min, and finally re-heated to 330 °C at 10 °C/min. The melting temperature (T_m) and enthalpy change (ΔH_m) during the second heating step were measured to determine the degree of crystallinity (X_c) of the blends, employing the following equation:

$$X_c(\%) = \frac{\Delta H_m}{\Delta H_m^0 \cdot (1 - f_w)} \cdot 100 \quad (1)$$

where $\Delta H_m^0 = 240$ J/g represents the melting enthalpy per gram of 100 % crystalline nylon 6 polymer (average between α-phase - 241 J/g and γ-phase - 239 J/g, respectively [50]), and f_w denotes the weight fraction of the biochar in the blend, rescaled on the residue at the end of thermal analysis in air. The DSC curves presented in the manuscript refer to the second heating step.

To evaluate the thermal stability of the pristine materials and blends, thermogravimetric analysis (TGA) was performed on the pellets using a STA 2500 Regulus instrument by Netzsch GmbH (Selb, Germany). Approximately 15 mg of each sample was placed in a platinum pan and subjected to heating from room temperature to 900 °C at a rate of 10 °C/min under a nitrogen atmosphere (50 ml/min), followed by heating to 1300 °C in air at the same rate. Further TGA was conducted to examine the thermal degradation kinetics of nylon 6-biochar blends. To this aim, the Flynn-Wall-Ozawa (FWO) Eq. (2) was used to determine the activation energy (E) that must be overcome for the combustion reaction to proceed [48,51]:

$$\log(\beta) = -2.315 - 0.457\frac{E}{RT} \quad (2)$$

where β denotes the heating rate, T is the temperature (K), and R is the universal gas constant. The equation reveals that the variable log (β) exhibits a linear correlation with the variable $1/T$. Therefore, the activation energy E corresponding to a given level of degradation can be derived by calculating the slope of the log (β) versus $1/T$ graph. Subsequently, the average activation energy was calculated as the mean value obtained from each conversion. FWO thermogravimetric analyses were performed from room temperature to 900 °C in air (50 ml/min) at different heating rates, namely, 1, 5, 10, and 20 °C/min.

2.3.3. Morphology

The morphology of the biochar samples was analysed using a Quanta FEG 450 Scanning Electron Microscope (SEM) equipped with Energy Dispersive Spectroscopy (EDS) by FEI Inc (Hillsboro, USA). Before analysis, the biochar powders were sputter-coated with a thin layer of gold using an Edwards Sputter Coater S150B apparatus.

Field Emission Scanning Electrical Microscopy FE-SEM, Zeiss SupraTM 25 (Oberkochen, Germany) operating at 5 keV was employed to analyse the morphology of composites.

2.3.4. Water absorption analysis

The water uptake of blend granules was evaluated following the ASTM D570 standard. Three sample replicates were prepared and desiccated until constant weight before starting the tests. Each sample was weighed every 24 h over a total period of 30 days using a precision weight balance with an accuracy of 0.0001 g. The water uptake W_{abs} was calculated using Eq. (3):

$$W_{abs}(\%) = \frac{W_1 - W_0}{W_0} \cdot 100 \quad (3)$$

where W_1 and W_0 are the wet and dry weights of the blends, respectively. The corresponding percentage change in density of P', PRHX, and PBX granules was measured at 20 °C using a 50 ml pycnometer and deionized water as liquid medium.

2.3.5. Rheological analysis

The effect of biochar on the rheological behaviour was assessed at 250 °C using a MCR 92 Rheometer by Anton Paar (Graz, Austria), employing a plate-plate geometry featuring a 25 mm diameter and 1 mm gap. Initially, an amplitude sweep test (from 0.01 % to 100 %) was carried out with a fixed angular frequency $\omega = 10$ rad/s to determine optimal operational parameters for identifying the linear viscoelastic limit. Then, oscillatory frequency sweep tests ranging from 0.05 to 100 Hz (0.314–628 rad/s) were performed with a fixed shear strain (0.2 %). The complex viscosity (η^*), and the loss factor ($\tan\delta$) were evaluated as a function of angular frequency (ω).

2.3.6. Mechanical tests

Tensile tests were conducted according to the UNI 527–2 standard, using type 5 A dog-bone specimens. For this purpose, dog-bone specimens were injection-moulded at 250 °C using a Megatech HD 22–50 press by Tecnica Duebi Srl (Ancona, Italy). The samples were then kept at 80 °C for an additional minute before being extracted from the mould. Stress-strain testing was carried out at room temperature using a Quasar 10 system machine by Galdabini Srl (Varese, Italy) equipped with a 1 kN load cell. Each test was performed on 5 specimens at a crosshead speed of 10 mm/min, and mean values along with relative standard deviations were subsequently reported.

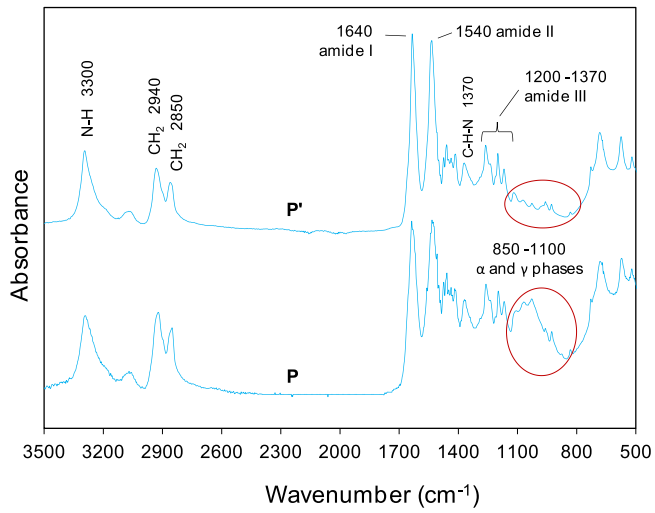

Fig. 1. FT-IR spectra of nylon 6 virgin fishing net (P) and processed fishing net (P').

3. Results and discussion

3.1. FT-IR and raman spectroscopy

To evaluate the impact of thermal processing on the recycling of fishing nets, virgin net granules were extruded under the processing conditions outlined in Section 2.2. The structural characterization of the samples was conducted through FT-IR analysis (Fig. 1). Both unprocessed (P) and processed (P') nets were analysed, normalizing their spectra to the band at around 1370 cm^{-1}, which corresponds to the bending vibration of the C-N-H bond [12]. The FT-IR spectrum of the virgin sample (P) exhibits characteristic bands of polyamide 6, namely: a peak around 3300 cm^{-1} attributed to hydrogen-bonded N-H stretching [12], peaks at 2940 and 2850 cm^{-1} associated with methylene CH_2 stretching vibration [12], sharp peaks at approximately 1640 and 1540 cm^{-1} corresponding to amide I C═O stretching and amide II N-H bending, respectively, and bands in the amide III region between 1370 and 1200 cm^{-1}. Comparatively, the processed sample P' exhibits similar peaks to the virgin one, with overlapping spectra except in the 1100 and 850 cm^{-1} region, where multiple bands appear due to monoclinic α and γ crystal phases of polyamide 6 [52,53]. Specifically, the band at 930 cm^{-1} is associated with the α crystal phase of polyamide 6, while the band at around 973 cm^{-1} is related to the γ crystal phase [52,53]. The processed sample (P') exhibits less pronounced peaks in the 1100–850 cm^{-1} region compared to the unprocessed sample (P), which may be elucidated by the findings of Mondragon et al. [12]. In particular, the authors combined FT-IR with XRD analyses and demonstrated that mechanical and thermal processing at temperatures exceeding 250 °C alters the α to γ ratio during recrystallization/cooling at room temperature, thereby affecting the peak proportion in the 1100–850 cm^{-1} range. This explains the difference in peak intensity between P and P' within this spectral region.

The FT-IR spectra of the PRHX and PBX blends reported in Fig. 2 indicate the absence of specific molecular interactions between P' and both RH and B biochar, which act as inert fillers. While Ogunsona et al. [54] suggested that strong interfacial adhesion between biocarbon and polyamide could be attributed to potential hydrogen bonding, the spectrum comparison between the processed virgin net P' and PRHX and PBX blends reveals negligible chemical shifts or the appearance of additional bands indicative of chemical bonding between the filler and the polyamide matrix. Notably, biochar, being predominantly carbon-based, lacks distinct absorption bands within the 4000–650 cm^{-1} range. The B and RH spectra roughly overlap, except for the 900–1200 cm^{-1} region (Fig. 3). The intense band at 1055 cm^{-1} corresponds to the stretching vibrations of silicon-oxygen tetrahedrons as SiO_4 and denotes a high silica content of RH [55]; conversely, the very low silica content in B does not allow for detecting Si-O signal in the corresponding FT-IR spectrum.

Fig. 4a and Fig. 4b show the deconvoluted Raman spectra of typical B and RH biochars in the characteristic region that allows for the

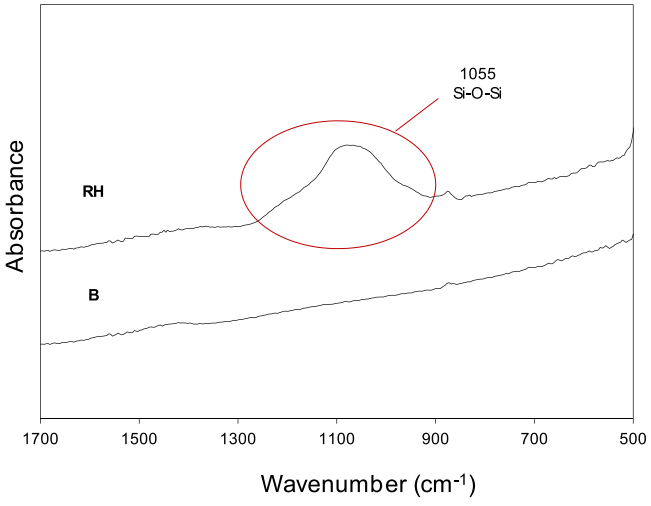

Fig. 3. FT-IR spectra of B and RH biochars.

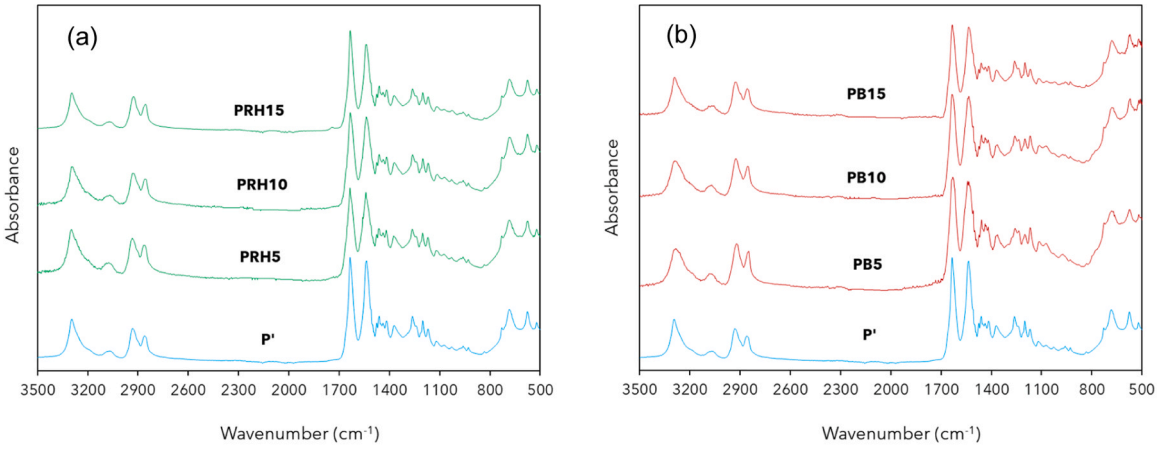

Fig. 2. FT-IR spectra of P', PRHX (**a**), and PBX (**b**) blends.

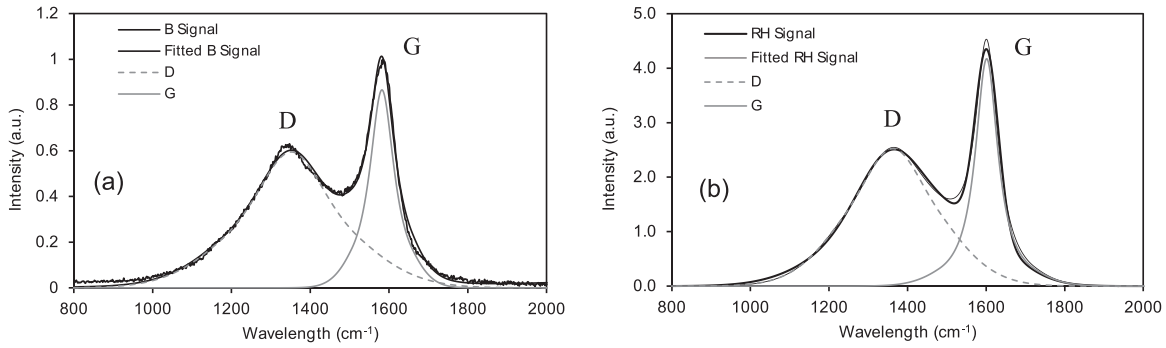

Fig. 4. Raman spectrum of B (**a**) and RH (**b**) biochars in the 800–2000 cm^{-1} range.

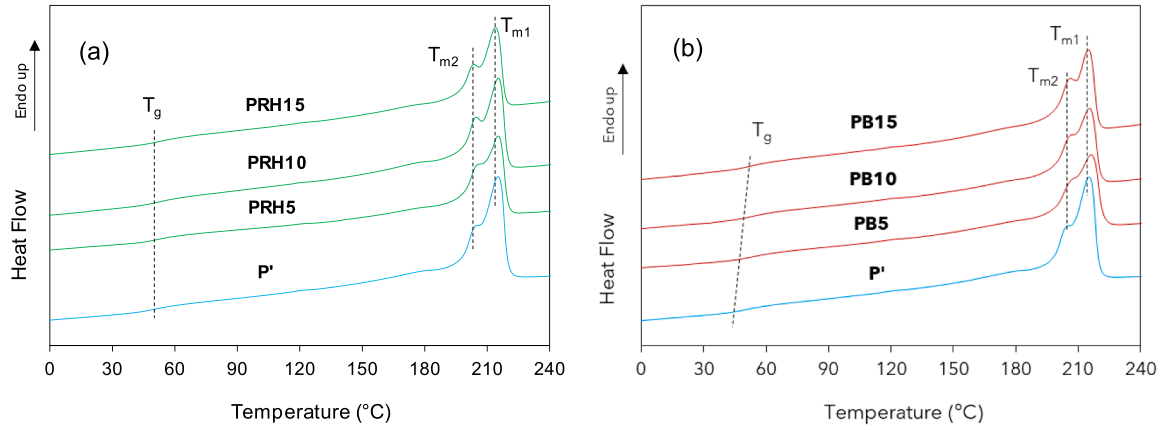

Fig. 5. DSC thermograms of P', PRHX (**a**), and P', PBX (**b**). 2nd heating scan = 10 °C/min from −50 °C to 330 °C.

Table 1
Melting temperature (T_{m1}, T_{m2}), glass transition temperature (T_g), and degree of crystallinity (X_c) of P', PRHX (**a**), and P', PBX (**b**).

Sample	T_{m1} (°C)	T_{m2} (°C)	T_g (°C)	X_c (%)
P'	214.5	205.0	48.3	21.7
PB5	214.0	206.0	48.5	22.9
PB10	216.0	205.5	51.7	25.8
PB15	215.5	206.0	55.8	32.1
PRH5	215.0	205.0	48.3	21.9
PRH10	215.5	206.0	48.1	22.3
PRH15	215.5	205.5	48.4	21.6

quantification of crystallite size of pyrolytic graphite [56]. Both plots display intense D and G peaks centred respectively at about 1350 and 1600 cm^{-1} and a not well-structured 2D region in the 2300–3500 cm^{-1} range, which is not reported here for the sake of clarity. The I_D/I_G ratio is approximately 2.4 (B sample) and 3.6 (RH sample), suggesting the presence of a highly disorganized sp^2 carbon structure, as evidenced by the small volumetric crystallite size of up to around 24.7 Å and 12.2 Å, respectively [56]. This is consistent with the low temperature of pyrolysis used to produce RH, which did not allow for a turbostratic rearrangement of graphitic crystallites, as reported by Torsello et al. for temperatures exceeding 800 °C [57].

3.2. Thermal characterization

3.2.1. Differential scanning calorimetry (DSC)

The DSC thermograms reported in Fig. 5, corresponding to the second heating scan at 10 °C/min, support for the presence of both α and γ crystal phases previously discussed. The α form appears as the more

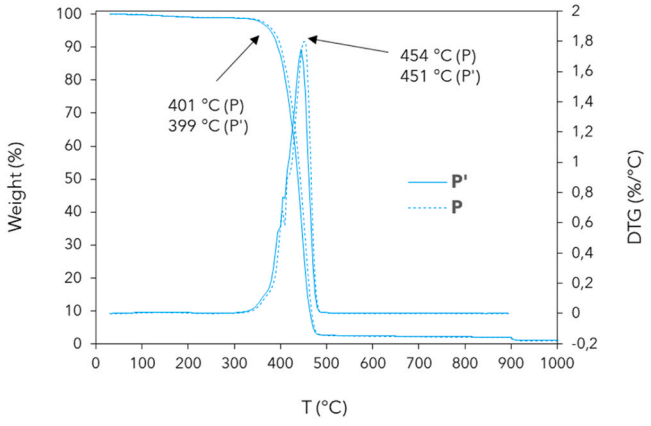

Fig. 6. TG and DTG curves of virgin (P) and processed (P') fishing nets. Heating rate = 10 °C/min from room temperature to 900 °C in nitrogen, and from 900 °C to 1300 °C in air.

thermodynamically stable phase, evidenced by prominent peaks (T_{m1}) in the 214–216 °C range, whereas the γ metastable form is visible as a minor shoulder peak at lower temperatures (T_{m2}) at about 205–206 °C. All P', PBX, and PRHX samples exhibit melting temperatures (T_{m1} and T_{m2}) comparable to those reported in the literature [58,59]. The consistency of melting temperatures suggests that none of the fillers preferentially induces the formation of a specific polymorph over the other. Conversely, the observed increase in glass transition temperature (T_g) and degree of crystallinity (X_c) of PBX blends suggests a stronger affinity between the polyamide matrix and biochar type B compared to RH

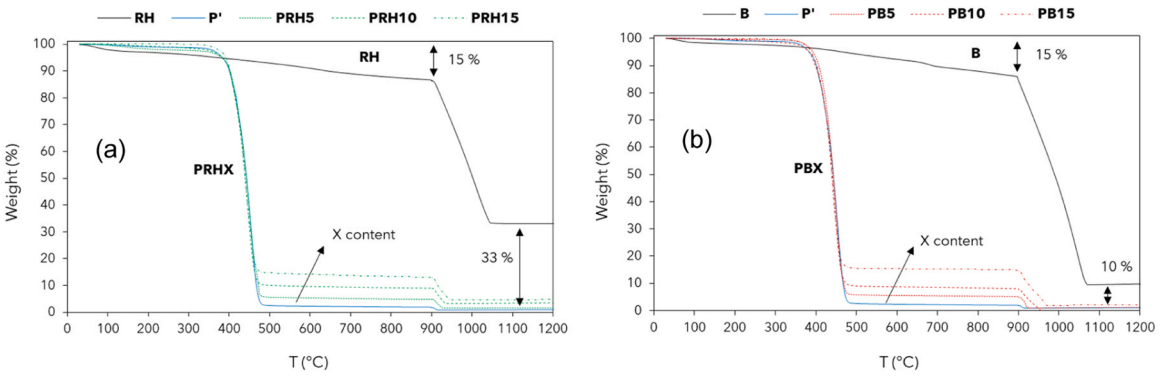

Fig. 7. TGA curves of P', PRHX (**a**), and P', PBX (**b**). Heating rate = 10 °C/min from room temperature to 900 °C in nitrogen, and from 900 °C to 1300 °C in air.

(Table 1). T_g ranges from 48.3 to 55.8 °C, and X_c varies from 21.7 % to 32.1 % with the addition of B, whereas they remain relatively constant with RH incorporation, comparable to pure P'. It is hypothesized that different biochars may interact diversely with the polyamide matrix. Particularly, oxygen-rich biochars present carboxyl, hydroxyl, and carbonyl groups, which can form hydrogen bonds, not clearly detectable via FT-IR, with the amide groups of polyamide 6, thus enhancing interfacial adhesion between biocarbon and polyamide [54,60]. Hence, the more compatible B filler tends to interact favourably with the polymer chains, restraining their mobility and thereby increasing the T_g of the blend material. Additionally, the B filler can act as a nucleating agent, facilitating the formation of crystalline domains within the polymer matrix, leading to an increase in the degree of crystallinity (X_c).

3.2.2. Thermogravimetric analysis (TGA)

The TGA curves reported in Fig. 6 confirm the findings of the previous FT-IR spectra (Fig. 1). Both unprocessed P and processed P' nets exhibit nearly identical thermal degradation profiles, indicating that extrusion processing did not degrade the polymer matrix significantly. Besides, slight deviations in the temperature onset and degradation peak from 401 °C (P) to 399 °C (P'), and from 454 °C (P) to 451 °C (P'), respectively, suggest minimal polymer fragmentation during the extrusion process. This implies the potential for efficient recycling and compounding of the virgin nets into new polyamide-biochar blends.

B and RH biochars exhibit a comparable degradation behaviour with a slow mass decay of about 15 wt% from room temperature up to 900 °C in nitrogen atmosphere (Fig. 7). This gradual decrease primarily stems from the presence of refractory organic substances and the inherent resistance of aromatic rings, such as degraded lignin, and robust C-C covalent bonds. The observed B and RH thermograms are indicative of carbonized materials derived from agricultural and forestry residues that underwent graphitization due to pyro-gasification processes [61]. In air atmosphere, rice husk biochar (RH) exhibits a greater residue (33 wt%) compared to lignocellulosic biochar (B) (10 wt%), thereby confirming the substantial presence of inert amorphous silica [32,40–43,62].

PRHX and PBX blends showed very similar degradation profiles with consistent thermal stability up to about 380–385 °C, which is compatible with the extrusion conditions adopted. All curves showed a single sharp mass decay with decomposition peaks at around 445–450 °C and asymptotic values in the nitrogen atmosphere, which roughly corresponds to the concentrations of biochar filler introduced into the blends (5, 10, and 15 wt%). This result confirms the effective dispersion of the biochars within the blends. Interestingly, PRHX presents final residues of 4–5 wt% in the oxidizing atmosphere compared to the PBX residues (1–2 wt%), which aligns with the greater presence of inert silica and other inorganic compounds based on Al, Cu, Fe, and Zn [43].

3.2.3. Flynn-Wall-Ozawa (FWO) degradation kinetics

To deepen our understanding of the degradation behaviour of the formulated PBX and PRHX blends, and to elucidate the impact of biochar on the initial temperature onset and degradation peak, additional thermogravimetric experiments were conducted under oxidative conditions. Specifically, we employed the Flynn-Wall-Ozawa (FWO) method outlined in Section 2.3.2 [48,51], which involves assessing mass loss at various heating rates to determine the activation energy (E) of the blends.

The impact of biochar was evaluated by comparing the activation energy of P' to that of the blends obtained at the highest biochar content (i.e., PRH15 and PB15), where the influence of biochar is mostly pronounced. The TGA analyses carried out at heating rates of 1, 5, 10, and 20 °C/min are reported in Fig. 8(a-c). The corresponding fittings derived from the kinetic plots at the conversion of 5, 10, 20, and 50 % are presented in Fig. 8(d-f). The selection of conversion up to 50 % was guided by the constraint that the FWO method applies only to well-resolved single-step decompositions and first-order kinetics degradation. All the TGA curves reported in Fig. 8 exhibit decomposition shoulders; hence, the evaluation of activation energy (E) was focused on the initial phase of the TGA curves (conversion < 50 %) where the FWO method remains valid and biochar predominantly exerts its thermal shielding effects [47,48].

The thermogravimetric analysis profiles showed a notable shift in degradation curves toward higher temperature ranges with increasing heating rates, indicating elevated decomposition temperatures due to reduced exposure time [46,63].

P' and PB15 exhibited similar activation energies ranging between 27.0 and 30.5 kJ mol^{-1} at low conversions (5 and 10 %), approximately half of those observed for PRH15 (~ 55 kJ mol^{-1}) under identical conditions. However, this discrepancy diminishes at higher conversions (20 and 50 %), suggesting that RH biochar provides superior protection against polymer thermal degradation during the initial stages. The average activation energy varied from 43.6 kJ mol^{-1} for P' to 53.0 kJ mol^{-1} and 70.9 kJ mol^{-1} for PB15 and PRH15, respectively, highlighting thermal-shielding properties, particularly for RH biochar. Indeed, the higher activation energy for PRH15 compared to P' implies a mechanism of thermal shielding, likely due to the high silica content of RH acting as an inert filler, isolating the polymer matrix and reducing its thermal degradation [28,39]. It has been demonstrated that as the heating process progresses, in this case, organic components undergo gradual decomposition and gasification, leaving silica as the predominant residue. The continuous accumulation of these silica residues ultimately results in the formation of a silica-ash layer, which acts as an effective heat shield, slowing down the heat and mass transfer involved in the degradation process [39].

The second stage of weight loss, as depicted in Fig. 9, highlights the appearance of shoulders attributed to the oxidation of the carbon skeleton remaining after the initial decomposition of both matrix and

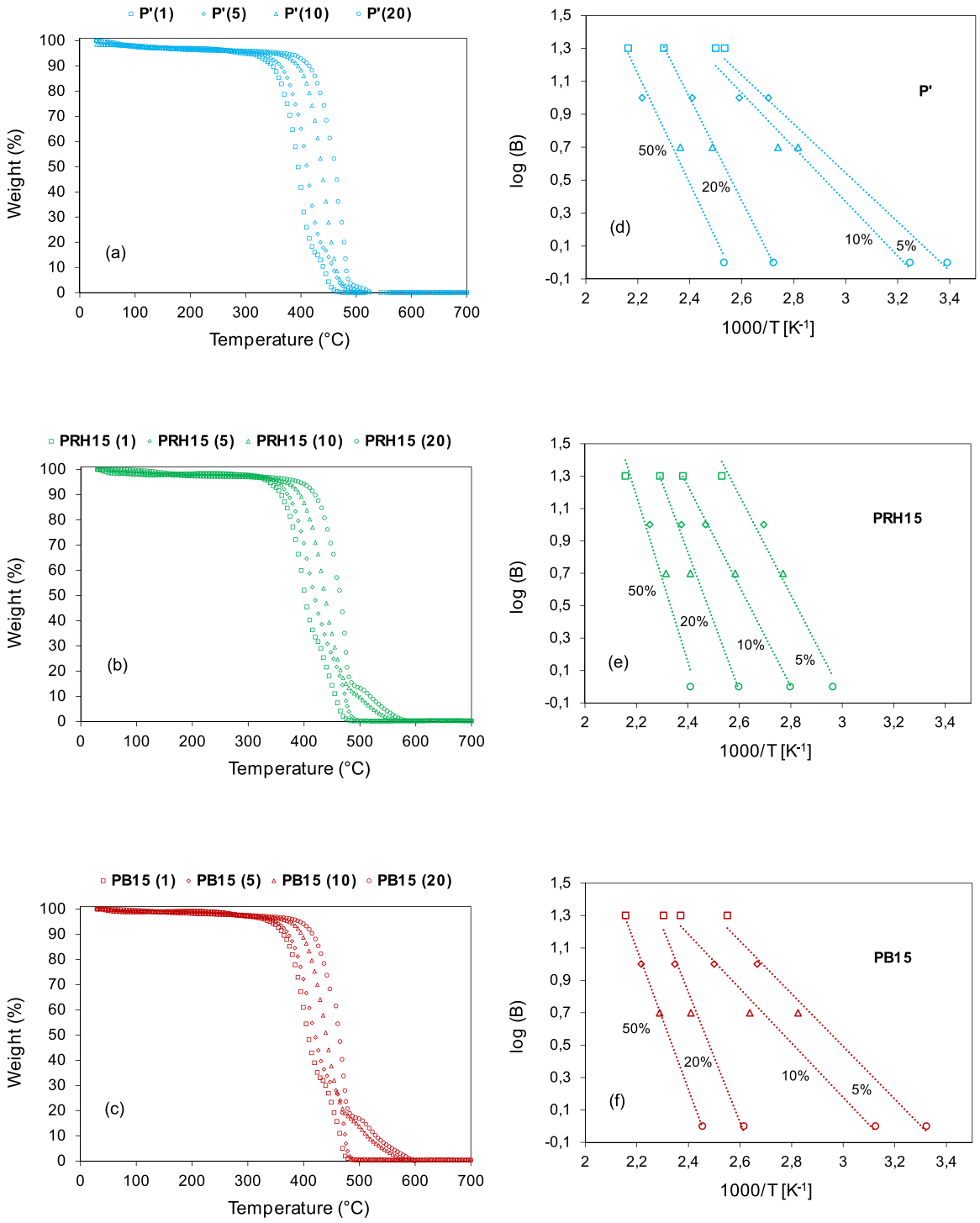

Fig. 8. TGA curves and kinetic plots of P' (**a,d**), PRH15 (**b,e**), and PB15 (**c,f**). Heating rate = 1 °C/min, 5 °C/min, 10 °C/min, and 20 °C/min from room temperature to 900 °C in air. Conversion = 5 %, 10 %, 20 %, and 50 %.

biochar. It has been postulated that the rate of oxidation is influenced by the heating rate; slower rates (1 °C/min) lead to the formation of a more porous carbon skeleton, facilitating faster oxidation, while faster rates (20 °C/min) result in less porous carbon skeletons and slower oxidation phenomena [64].

3.3. Water absorption characterization

The EDS microanalysis depicted in Fig. 10 showed a comparable concentration of atomic oxygen in both B and RH biochar samples (i.e., around 13–14 wt%). This oxygen is primarily present in functional groups such as COOH, OH, and C=O, as well as in silica (SiO_2) [65]. Given that RH biochar contains a Si concentration of 6 wt%, twice that of B biochar (3 wt%), the latter likely exhibits a higher abundance of carboxyl, hydroxyl, and carbonyl groups available for hydrogen bond formation with the amide groups of polyamide 6. This finding confirms the greater affinity observed through previous DSC analyses of B compared to RH when both are dispersed in the polyamide matrix. Additionally, the higher Si concentration supports the selection of RH filler as an effective thermal shield in recycled nylon 6-based fishing

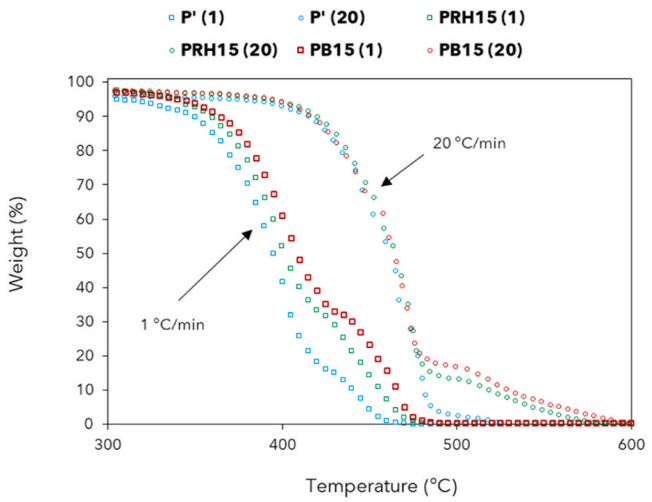

Fig. 9. TGA curves of P', PRH15, and PB15 at 1 and 20 °C/min. Heating rate = 1 °C/min and 20 °C/min from Troom to 900 °C in air.

nets. Furthermore, EDS results demonstrate the uniform distribution of other inorganic trace elements, including Fe, Na, K, and Ca, with concentrations ranging from 0.1 to 0.6 wt%.

The relatively high silica content present in RH biochar and its PRH15 blend compared to their respective B and PB15 counterparts is indirectly confirmed by the water absorption tests shown in Fig. 11. The results indicate the highest water absorption for neat P', reaching approximately 3.6 % over 30 days. This can be attributed to the strong polarity of polyamide 6 molecular chains, stemming from the presence of amide groups (–NHCO–), which exhibit significant hydrophilicity [54,66]. In contrast, biochar fillers typically possess hydrophobic properties; thus, their integration into the polyamide matrix decreases the overall material's affinity toward water. Therefore, an increase in biochar loading typically results in reduced water uptake. The findings in Fig. 11 were obtained with the highest biochar content (15 wt%), where the impact of biochar is most pronounced. The results demonstrate diminished water absorption for both PRH15 and PB15 compared to P', with values of 2.5 % and 1.8 % for PRH15 and PB15, respectively. Besides, it is worth noting that our water absorption results are lower than those achieved by Ogunsona et al. [54] in virgin polyamide 6 and miscanthus-based biochar, and numerically align with those obtained by Zhu et al. [50], who utilized virgin polyamide 6 matrix and bamboo-derived biochar. Zhang et al. (2020) demonstrated that high content of biochar (up to 70 wt%) may also negatively affect water absorption due to inadequate adhesion between the matrix and the polyethylene filler [32]. Similar outcomes were reported by Prabhu et al. in their investigation of biochar-epoxy composites [21]. Our results confirm the moisture-shielding effect provided by the biochars in the recycled polyamide matrix. Furthermore, the notably higher values observed for PRH15 may be attributed to the noticeable silica content

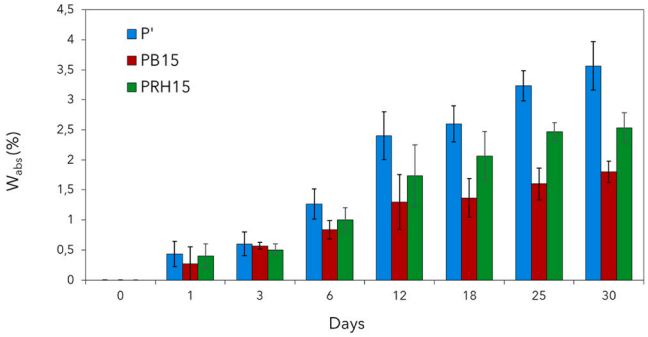

Fig. 11. Water absorption rate of P', PRH15, and PB15 blends.

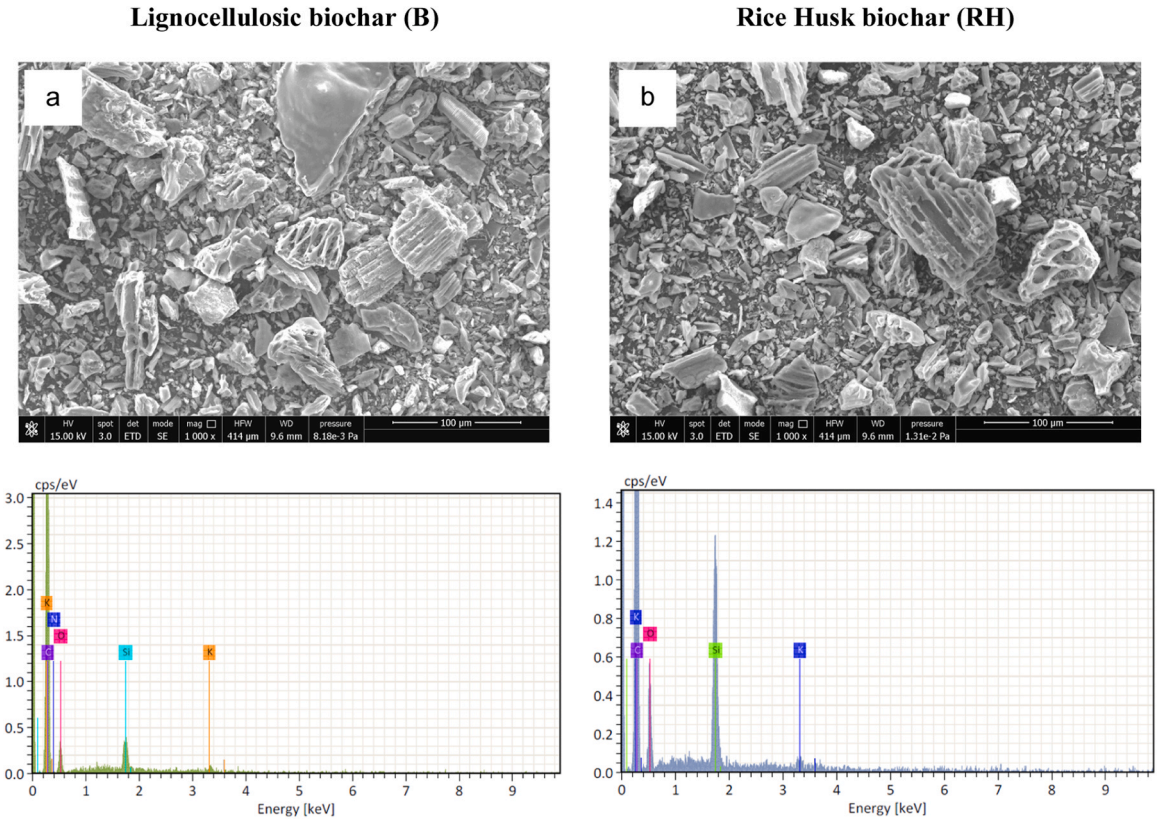

Fig. 10. SEM images and EDS microanalysis of lignocellulosic biochar B (**a**) and rice husk biochar RH (**b**).

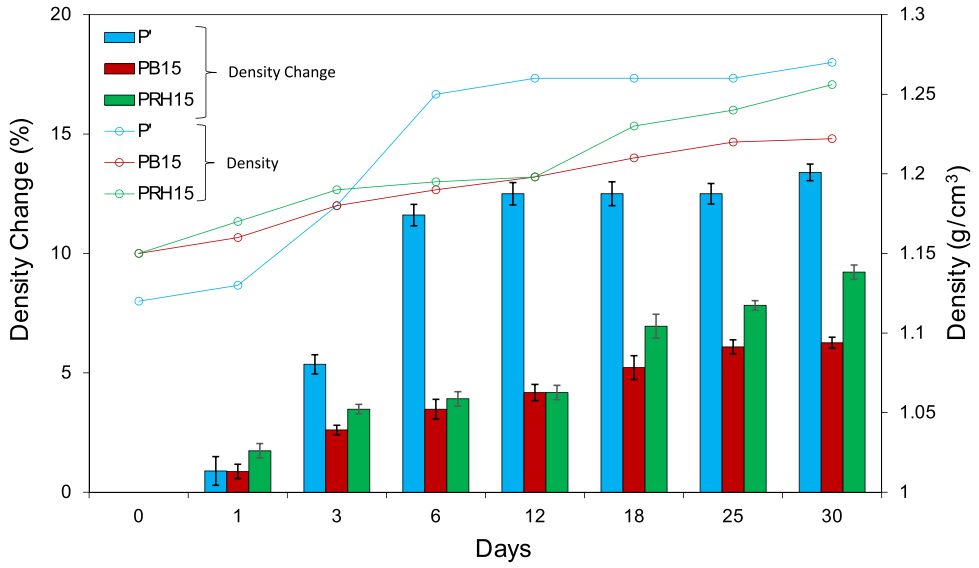

Fig. 12. Percentage change in density of P', PRH15, and PB15 blends.

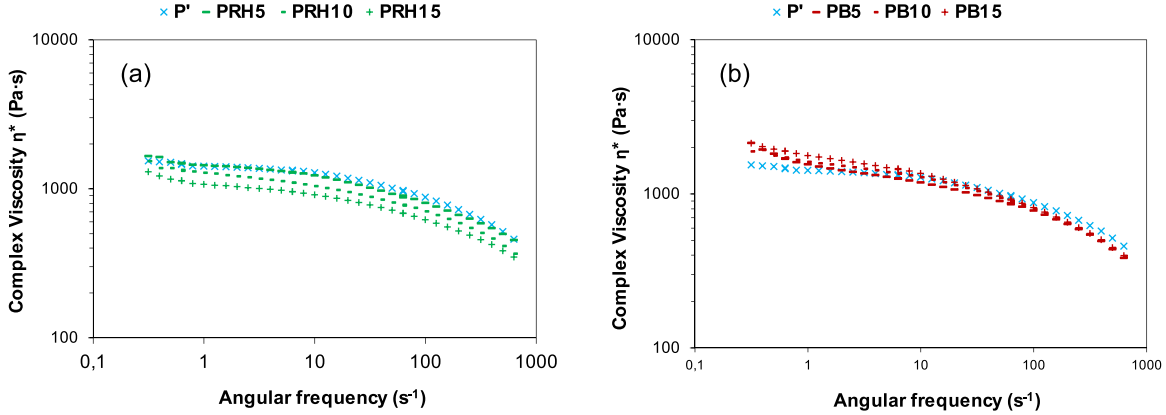

Fig. 13. Complex viscosity (η^*) versus angular frequency (ω) of P', PRHX (**a**), and P', PBX (**b**) blends at 250 °C.

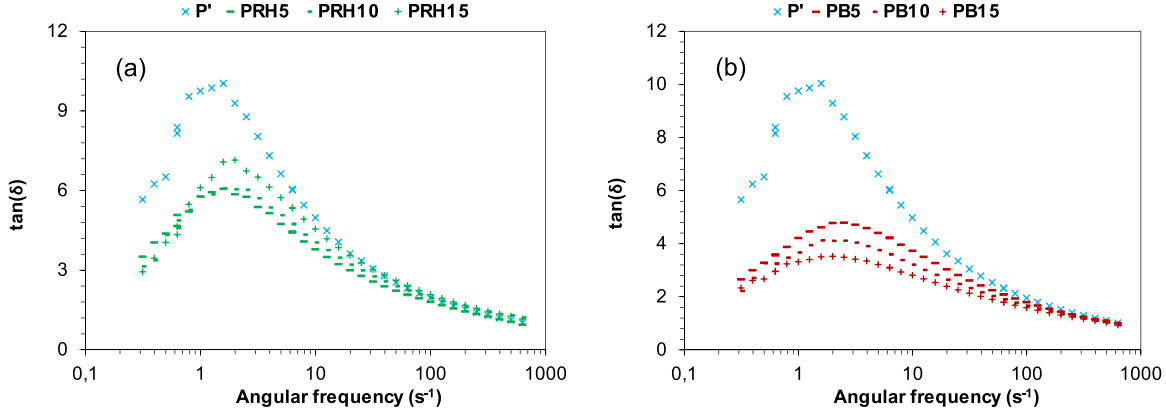

Fig. 14. Damping factor (tan δ) versus angular frequency (ω) of P', PRHX (**a**), and P', PBX (**b**) blends at 250 °C.

and the presence of silanol groups (Si-OH), which are particularly hydrophilic, thereby making PRH15 blend more hydrophilic than PB15. Conversely, the oxygen-rich groups in B tend to preferentially form hydrogen bonds with the amide groups of polyamide 6, thereby reducing their availability for water absorption [54,66].

To further validate the protective effect conferred by the biochars, Fig. 12 displays the density trends over time for P′, PB15, and PRH15. These trends corroborate the earlier observations regarding water uptake. Specifically, P′ demonstrates consistently higher densities, ranging from 1.12 to 1.27 g/cm^3 (13.4 % increase), while PB15 ranges from 1.15 to 1.22 g/cm^3 (6.1 % increase), and PRH15 ranges from 1.15 to 1.26 g/cm^3 (9.6 % increase). Both blends show lower water uptake compared to

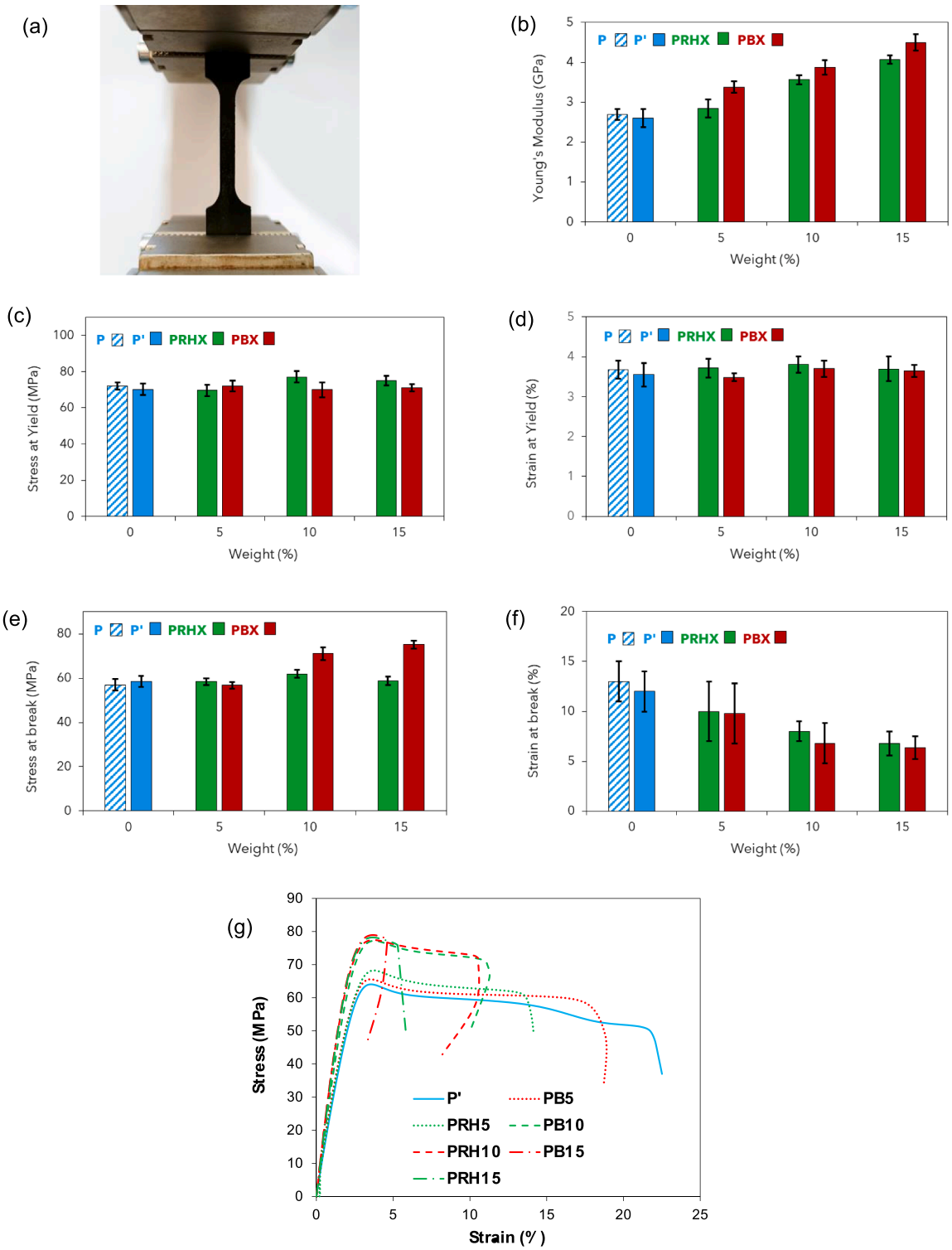

Fig. 15. Mechanical properties of P, P', PRHX, and PBX samples. Tensile testing configuration (**a**). Young's modulus (**b**), stress at yield (**c**), strain at yield (**d**), stress at break (**e**), and strain at break (**f**). Representative stress-strain curves (**g**). Mean values ± standard deviations (2σ) based on 5 replicates reported on error bars.

unfilled nylon P', suggesting that the biochar particles act as a barrier. It has been demonstrated that they tend to concentrate absorbed moisture within their pores and at the interface with the nylon 6 [27]. The slight difference in density between P′ and both PRH15 and PB15 (1.12 versus 1.15 g/cm^3) is attributed to the biochar loading, which typically possesses a higher density (ranging from 1.3 to 2 g/cm^3) than the P′ matrix [67]. Conversely, the biochar used as an additive in nylon 6 has a lower density compared to other inorganic reinforcing fillers such as talc and carbonates (up to 3 g/cm^3) employed in combination with polyamides, thus representing a potential solution for the development of low-density blends for lightweight applications such as in the automotive sector [26].

Finally, after prolonged drying in an oven for 48 h at 90 °C, the water uptake values return to those observed initially, except for P' which shows a residual water uptake of roughly 5 % likely associated with the presence of bound water molecules within the amorphous phase of

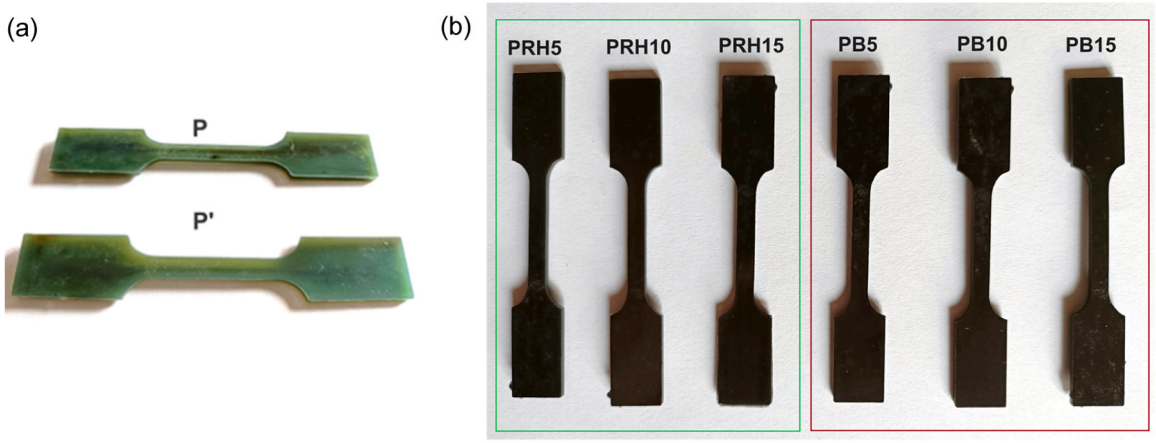

Fig. 16. Dog-bone specimens of P and P' (**a**), and PRHX and PBX blends (**b**).

nylon, which are more difficult to remove [27].

3.4. Rheological characterization

The influence of filler-matrix interfacial adhesion on the melting behaviour of blends is a well-established phenomenon in polymer science. Typically, strong interfacial adhesion effectively confines polymer chains around filler particles, thereby reducing polymer chain disentanglement and mobility. Conversely, weak adhesion results in minimal confinement and increased melt fluidity. The former behaviour leads to an increase in melt strength, melt flow index, and viscosity, while the latter results in a decrease in these rheological properties. Hence, to further investigate the interaction between the recycled nylon 6 and the incorporated biochars, the complex viscosity (η^*) and the damping factor ($\tan\delta$) were evaluated as functions of angular frequency (ω). The complex viscosity of P′ and its blends (PRHX and PBX) exhibited the characteristic rheological behaviour of shear-thinning fluids, where complex viscosity decreased with increasing angular frequency due to progressive chain disentanglement (Fig. 13). However, PRHX and PBX displayed different rheological behaviours. In particular, RH exhibited a fluidization effect, resulting in lower viscosities with increased RH content. This is likely due to the inadequate chemical bonding at the polymer-filler interface, along with the lubricating effect offered by the graphitic nature of the biochar and the partial degradation of its lignocellulose material into low molecular weight fractions [25,68]. In contrast, B showed a reinforcing effect, resulting in slightly higher viscosities with increased B loadings [54]. This suggests a minor fluidization effect that is also compensated by the char-polymer interaction caused by the oxygen-rich groups (i.e., hydrogen bonding) previously discussed.

Typically, increasing the filler content of polymer blends results in increased storage moduli over loss moduli. However, globally reduced damping factors were observed for both PRHX and PBX compared to P′ (Fig. 14). Nonetheless, the damping factor increased with RH loading, which confers fluidity to the melt, while it decreased with B loading, improving polymer-filler adhesion. The peaks in the damping factor reveal the effect of chain mobility restriction toward oscillation and, in particular, the threshold between viscous and elastic relaxation [69]. These peaks are all positioned at about $\omega^* = 2\ s^{-1}$ in all blends but are lower in PRHX than in PBX, confirming the lubrication/fluidizing effect of RH and the stiffening effect of B on the recycled nylon nets.

3.5. Mechanical characterization

To assess the mechanical performance provided by the incorporation of biochar fillers under typical operating temperatures, stress-strain tensile tests were conducted on P, P', PRHX, and PBX dog-bone specimens (Fig. 15a-g). As shown in Fig. 15, the tensile properties of virgin nets (P) perfectly overlap with those of virgin nylon 6, extruded under the same conditions. This result confirmed previous FT-IR and TGA outcomes demonstrating that the recycled fishing net materials maintain their physical and mechanical properties, making them suitable for repurposing in secondary lifecycle applications. As expected, in accordance with existing literature, both biochar fillers lead to matrix stiffening [26,32,68,70,71]. In particular, the incorporation of biochar results in a significant increase in the Young's Modulus by over 70 %, from 2.6 GPa (unfilled polyamide 6) to 4.5 GPa for PB15 (Fig. 15b). This enhancement is more pronounced in PBX blends compared to PRHX blends, thus confirming the superior affinity of the lignocellulosic biochar B with the polyamide 6 matrix. These findings align with the recent study by Hoang et al. [28], which reported enhanced char-polymer interfacial bonding and improved stress transmission for both rice husk-based and wood-based biochar [28]. Both stress and strain at yield remained stable and comparable to those of the unfilled matrix for PRHX and PBX (Fig. 15c-d), indicating the potential for loading the polymer matrix with higher concentrations of biochar fillers without compromising its mechanical behaviour. However, the reinforcing effect imparted to the polyamide matrix by both types of biochars is evident at longer elongation time, when observing the trends of the stress and strain at break (Fig. 15e-f). This embrittling effect is typical of thermoplastic polymers like PP, PBSA, PLA, PA6, and PA66, loaded with wood-based carbonaceous fillers [29,54,61,68,70,72]. In our case, the addition of biochar up to 15 wt% leads to a more rigid material with strain at break reduced by half (from 12.0 % for P', to about 6.8 % and 6.3 % for PRH15 and PB15, respectively). The higher interfacial adhesion between the biochar B filler and the matrix is further demonstrated by the higher values of stress at break measured in PB10 and PB15 compared to PRH10 and PRH15 counterparts (Fig. 15e).

The mechanical results were analysed using JMP Statistical Software with a one-way analysis of variance (ANOVA). The statistical analysis indicated significant differences in all mechanical properties among blends with different biochar loadings ($p < 0.05$).

3.6. Morphological characterization

B and RH biochar show an additional benefit through their natural pigmentation, making them viable renewable and cost-effective alternatives to fuel-derived carbon black pigments [68,73]. As depicted in Fig. 16, nylon 6/biochar blends display uniform macroscopic black coloration and consistent pigmentation, accompanied by qualitatively smooth and clean surfaces, regardless of the filler content incorporated into the recycled polyamide matrix.

The major interaction between biochar and polyamide appears to be primarily mechanical, with the polymeric matrix filling the micrometric

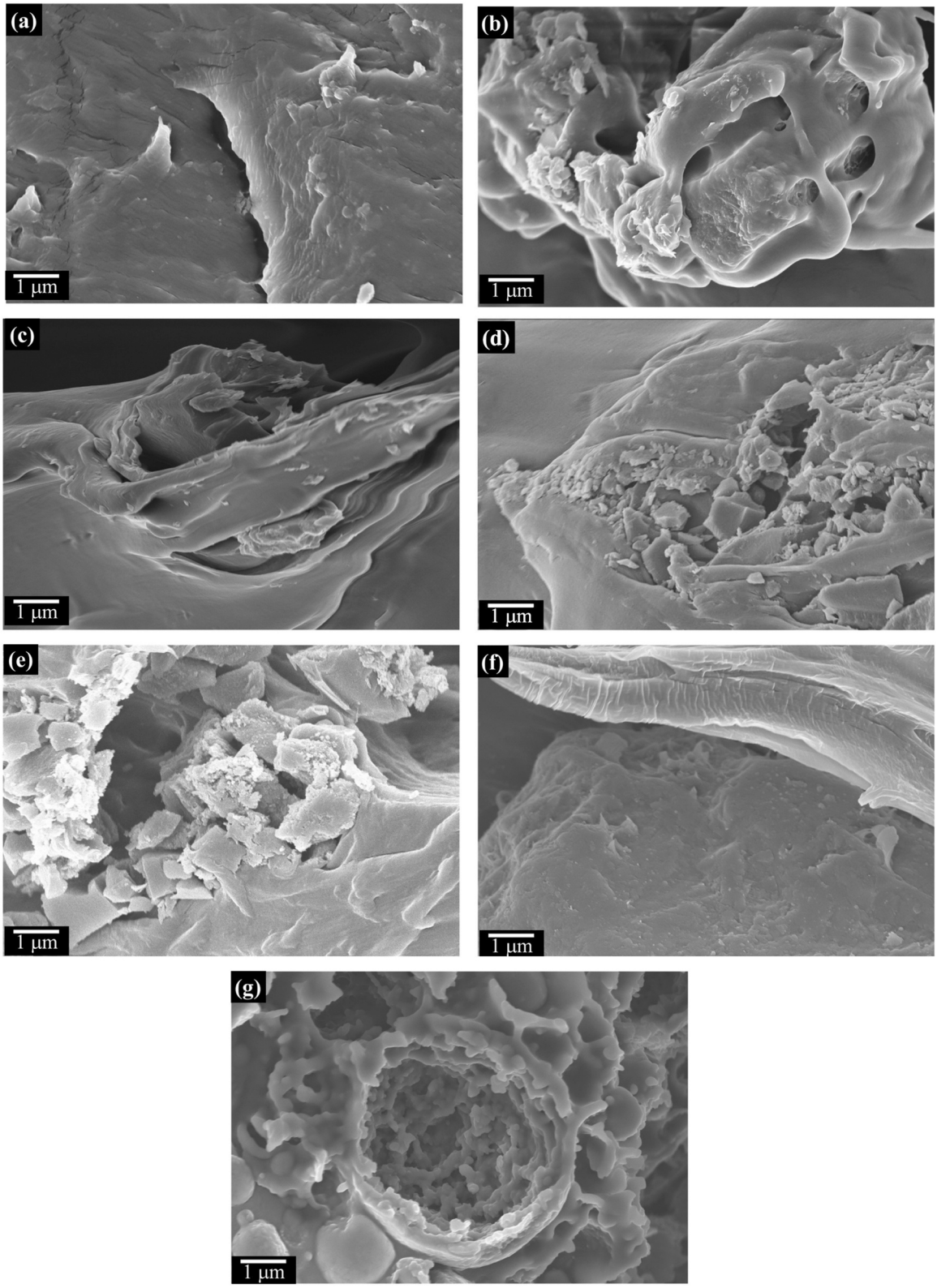

Fig. 17. FE-SEM images of neat P' (**a**), PB5 (**b**), PB10 (**c**), PB15 (**d**), PRH5 (**e**), PRH10 (**f**), and PRH15 (**g**).

porous network of biochar particles. As shown in figure Fig. 17a, the fracture of neat P' presents a relatively smooth surface; notable topological changes occur when biochar is embedded in the polymer matrix. PB5 and PB10 (Fig. 17b and Fig. 17c, respectively) show a homogeneous incorporation of biochar lamellar particles; however, when their loading increases up to 15 wt% (PB15) (Fig. 17d), small islands of filler appear. These agglomerates could be responsible for the embrittling and stiffening effect observed in the PBX blends compared to the PRHX blends (Fig. 15). The morphology of PB15 blends accounts for the interaction between B with the polymer matrix considering that the temperature used for biochar production promotes the aggregation of B biochar particles as shown in figure Fig. 17d. This phenomenon is likely to be

due to the π−π stacking interaction of carbon species. The different morphologies of RH-derived biochar play a key role as shown in Fig. 17e-g, where the polymeric matrix permeates the porous structure of RH biochar [23]. This morphology is formed through an appropriate balance of size and processing procedures, and does not occur in biochars like those derived from coffee, whose porous network collapses, as demonstrated by Arrigo et al. [74]. As clearly shown in figure Fig. 17 g, RH biochar exhibits a more porous morphology with fewer lamellar structures; its pores are fully filled with the polymer matrix, preventing the clustering phenomenon previously observed [75]. Further, RH-derived biochar contains a significant amount of silica (Fig. 3), which contributes to moisture retention (Fig. 11). This makes RH less available to form hydrogen bonds with polyamide moieties, thereby offering slightly lower mechanical performance than B-derived blends (Fig. 15).

4. Conclusions

This study investigates the development of an innovative, sustainable polymer-modified material composed of a polyamide 6 (PA6) matrix and a biochar filler, derived from recycled PA6 fishing nets and the pyrolysis of vegetable waste, respectively. The circularity of this newly developed material is achieved through the reuse of a polymeric matrix, which currently lacks a dedicated recycling system and is often improperly discarded in seas or landfills. The material's sustainability is further enhanced by the use of biochar as a substitute for carbon black pigment. Biochar is more sustainable than carbon black, as it is produced from renewable biomass and contributes to carbon sequestration in the soil. In contrast, carbon black is derived from non-renewable fossil fuels, leading to higher CO_2 emissions and a greater environmental impact.

Two distinct types of biochar, namely lignocellulosic biochar (B) and rice husk biochar (RH), were employed as bio-based fillers to enhance the thermal and mechanical properties of the final blend materials. FT-IR, DSC, and mechanical tensile tests performed on the pristine recovered material demonstrated the efficient reprocessing of discarded fishing nets through melt extrusion with minimal modification/worsening of their characteristics. Subsequently, PA6/biochar blends were successfully compounded and tested using different biochar loadings.

DSC analysis elucidated a more pronounced interaction between biochar B and the polymer matrix compared to RH. In fact, biochar B acted as an effective nucleating agent, limiting polymer chain disentanglement, promoting crystallinity, and shifting the T_g toward higher temperatures. The presence of oxygen-rich groups (COOH, OH, and C═O) in biochar B facilitated favourable interactions with the polyamide matrix, resulting in the formation of hydrogen bonds with amide groups. This led to the formation of stiffer and less ductile blends characterized by an enhanced Young's modulus, increasing from 2.6 to 4.5 GPa compared to the virgin nets, higher tensile strength, and reduced strain at break. Moreover, biochar B exhibited a moisture-shielding effect owing to its hydrophobic aromatic nature, resulting in a 30-day water uptake of 1.8 %, compared with 3.6 % for virgin nets, alongside a diminished density change from 13.4 % to 6.1 %. The reinforcing effect of biochar B yielded a marginal improvement in melt viscosity and processability.

Conversely, RH exhibited distinct properties due to its limited interaction with the PA6 matrix, stemming from its lower content of oxygen-rich groups. Consequently, RH manifested a lubricating effect, reducing polymer melt viscosity and improving processability, thereby exerting a minor influence on the degree of crystallinity and the mechanical properties compared to the B filler. Interestingly, RH showed substantial silica (SiO_2) content and demonstrated a superior affinity with water compared to B, leading to a water uptake of 2.5 % and a density variation of 9.6 %. The high silica content measured via SEM-EDS analysis conferred higher thermo-oxidative stability to RH/PA6 blends, as demonstrated by the increase in the activation energy for oxidation from 43.6 to 70.9 kJ mol^{-1}.

In summary, biochar B can be preferred for its superior mechanical strength and moisture-resistant characteristics, whereas RH is better as regards its thermo-oxidative stability. Both fillers can be integrated up to 15 wt% to replace conventional petroleum-derived carbon black pigments, thereby reducing the overall cost of PA6-based blends. Furthermore, both biochar fillers exhibit lower densities compared to traditional inert fillers like talc and carbonates, making them suitable for lightweight applications. Given the favourable overall mechanical and thermal performance of the designed blends, they could be suitable for applications requiring a balance of lightweight properties and adequate mechanical strength. In this context, the investigated blends could be exploited in the automotive industry, for the manufacturing of lightweight parts or components that are mechanically resistant and do not have to accumulate static electricity for safety reasons.

Funding

This research was financed by the European Union - NextGenerationEU (National Sustainable Mobility Center. CN00000023. Italian Ministry of University and Research Decree n. 1033–17/06/2022. Spoke 11 - Innovative Materials & Lightweighting - Scalability Project "SUSTAINED").

CRediT authorship contribution statement

Damiano Rossi: Writing – original draft, Methodology, Investigation, Formal analysis, Conceptualization. **Miriam Cappello:** Validation, Formal analysis, Data curation. **Maurizia Seggiani:** Writing – review & editing, Supervision, Project administration, Funding acquisition, Conceptualization. **Sara Filippi:** Visualization, Resources. **Mattia Bartoli:** Software, Formal analysis. **Giulio Malucelli:** Writing – review & editing, Funding acquisition. **Patrizia Cinelli:** Writing – review & editing, Project administration.

Declaration of Competing Interest

The authors declare that they have no known competing financial interests or personal relationships that could have appeared to influence the work reported in this paper.

Acknowledgements

The authors would like to acknowledge Irene Anguillesi for her support in carrying out the thermal and rheological tests and for her significant technical feedback and comments; Marco Sandroni for his important technical advice and great experience in processing the blends.

Data Availability

Data will be made available on request.

References

[1] Plastic Europe: Plastics - The Facts Available online: https://plasticseurope.org/knowledge-hub/plastics-the-facts-2022/.
[2] D.K.A. Barnes, F. Galgani, R.C. Thompson, M. Barlaz, Accumulation and fragmentation of plastic debris in global environments, Philos. Trans. R. Soc. B Biol. Sci. *364* (2009) 1985–1998, https://doi.org/10.1098/rstb.2008.0205.
[3] L. Peng, D. Fu, H. Qi, C.Q. Lan, H. Yu, C. Ge, Micro- and nano-plastics in marine environment: source, distribution and threats — a review, Sci. Total Environ. *698* (2020) 134254, https://doi.org/10.1016/j.scitotenv.2019.134254.
[4] L. Lebreton, B. Slat, F. Ferrari, B. Sainte-Rose, J. Aitken, R. Marthouse, S. Hajbane, S. Cunsolo, A. Schwarz, A. Levivier, et al., Evidence that the great pacific garbage patch is rapidly accumulating plastic, Sci. Rep. *8* (2018) 1–15, https://doi.org/10.1038/s41598-018-22939-w.
[5] J.D. Linton, R. Klassen, V. Jayaraman, H. Walker, S. Brammer, R. Ruparathna, K. Hewage, J. Thomson, T. Jackson, D. Baloi, et al., Evaluating scenarios toward

zero plastic pollution, Sci. (80-.) *369* (2020) 1455–1461, https://doi.org/10.1126/science.aba9475.
[6] Macfadyend Graeme, Huntington Tim, Rod cappell abandoned, lost or otherwise discarded fishing gear, FAO Fish. Aquac. *523* (2009) 115.
[7] Hanke, G.; Walvoort, D.; van Loon, W.; Maria Addamo, A.; Brosich, A.; del Mar Chaves Montero, M.; Eugenia Molina Jack, M.; Vinci, M.; Giorgetti, A. *EU Marine Beach Litter Baselines*; 2019;
[8] J. Pinto Da Costa, T. Rocha Santos, A. Duarte, The environmental impacts of plastics and micro-plastics use, waste and pollution: EU and national measures, Eur. Union (2020) 10–62.
[9] W.C. Li, H.F. Tse, L. Fok, Plastic waste in the marine environment: a review of sources, occurrence and effects, Sci. Total Environ. *566–567* (2016) 333–349, https://doi.org/10.1016/j.scitotenv.2016.05.084.
[10] A.L. Andrady, Microplastics in the marine environment, Mar. Pollut. Bull. *62* (2011) 1596–1605, https://doi.org/10.1016/j.marpolbul.2011.05.030.
[11] F. Vilaplana, S. Karlsson, Quality concepts for the improved use of recycled polymeric materials: a review, Macromol. Mater. Eng. *293* (2008) 274–297, https://doi.org/10.1002/mame.200700393.
[12] G. Mondragon, G. Kortaberria, E. Mendiburu, N. González, A. Arbelaiz, C. Peña-Rodriguez, Thermomechanical recycling of polyamide 6 from fishing nets waste, J. Appl. Polym. Sci. *137* (2020) 1–6, https://doi.org/10.1002/app.48442.
[13] C. Mihut, D.K. Captain, F. Gadala-Maria, M.D. Amiridis, Review: recycling of nylon from carpet waste, Polym. Eng. Sci. *41* (2001) 1457–1470, https://doi.org/10.1002/pen.10845.
[14] Patagonia NetPlus Available online: ⟨https://eu.patagonia.com/be/en/shop/collections/netplus⟩.
[15] Plastix Global Available online: ⟨https://plastixglobal.com/⟩.
[16] Y. Wang, Fiber and textile waste utilization, Waste Biomass-.-. Valoriz. *1* (2010) 135–143, https://doi.org/10.1007/s12649-009-9005-y.
[17] T. Srimahachota, H. Yokota, Y. Akira, Recycled nylon fiber from waste fishing nets as reinforcement in polymer cement mortar for the repair of corroded RC beams, Mater. (Basel) *13* (2020), https://doi.org/10.3390/MA13194276.
[18] CirculenRecover Available online: ⟨https://www.lyondellbasell.com/en/sustainability/circulen/⟩.
[19] ECONYL Available online: ⟨https://www.econyl.com/blog/fishing-nets-from-aquaculture-and-fish-industry-and-ghost-nets/⟩.
[20] Y. Cheng, A. Li, W. Shi, L. Zhao, Magnetic chitosan-functionalized waste carton biochar composites for efficient adsorption of anionic and cationic dyes, Chem. Eng. J. *481* (2024) 148535, https://doi.org/10.1016/j.cej.2024.148535.
[21] P. Prabhu, D. Jayabalakrishnan, V. Balaji, K. Bhaskar, T. Maridurai, V.R. A. Prakash, Mechanical, tribology, dielectric, thermal conductivity, and water absorption behaviour of caryota urens woven fibre-reinforced coconut husk biochar toughened wood-plastic composite, Biomass-.-. Convers. Biorefinery *14* (2024) 109–116, https://doi.org/10.1007/s13399-021-02177-3.
[22] N. Bolan, S.A. Hoang, J. Beiyuan, S. Gupta, D. Hou, A. Karakoti, S. Joseph, S. Jung, K.H. Kim, M.B. Kirkham, et al., Multifunctional applications of biochar beyond carbon storage, Int. Mater. Rev. *67* (2022) 150–200, https://doi.org/10.1080/09506608.2021.1922047.
[23] M. Bartoli, R. Arrigo, G. Malucelli, A. Tagliaferro, D. Duraccio, Recent advances in biochar polymer composites, Polym. (Basel) *14* (2022) 1–30, https://doi.org/10.3390/polym14122506.
[24] M. Giorcelli, A. Khan, N.M. Pugno, C. Rosso, A. Tagliaferro, Biochar as a cheap and environmental friendly filler able to improve polymer mechanical properties, Biomass-.-. Bioenergy *120* (2019) 219–223, https://doi.org/10.1016/j.biombioe.2018.11.036.
[25] T.A. Tengku Yasim-Anuar, L.N. Yee-Foong, A.A. Lawal, M.A. Ahmad Farid, M. Z. Mohd Yusuf, M.A. Hassan, H. Ariffin, Emerging application of biochar as a renewable and superior filler in polymer composites, RSC Adv. *12* (2022) 13938–13949, https://doi.org/10.1039/d2ra01897g.
[26] D. Jubinville, M. Abdelwahab, A.K. Mohanty, M. Misra, Comparison in composite performance after thermooxidative aging of injection molded polyamide 6 with glass fiber, talc, and a sustainable biocarbon filler, J. Appl. Polym. Sci. *137* (2020) 1–13, https://doi.org/10.1002/app.48618.
[27] E.O. Ogunsona, M. Misra, A.K. Mohanty, Accelerated hydrothermal aging of biocarbon reinforced nylon biocomposites, Polym. Degrad. Stab. *139* (2017) 76–88, https://doi.org/10.1016/j.polymdegradstab.2017.03.013.
[28] P. Hoang, Z. Zhang, J. Ren, Y. Peng, J. Cao, Versatile biochar for wood-plastic composites: improving mechanical properties, dimensional and thermal stability, Polym. Compos. *45* (2024) 10349–10364, https://doi.org/10.1002/pc.28477.
[29] S. Jurczyk, J. Andrzejewski, A. Piasecki, M. Musioł, J. Rydz, M. Kowalczuk, Mechanical and rheological evaluation of polyester-based composites containing biochar, Polym. (Basel) *16* (2024), https://doi.org/10.3390/polym16091231.
[30] S. Rajendran, G. Palani, K. Arunprasath, V. Shanmugam, U. Marimuthu, A. Veerasimman, Eco-friendly sugarcane biochar filler for enhanced mechanical properties in S-glass/polyester hybrid composites, Clean. Eng. Technol. *20* (2024) 100759, https://doi.org/10.1016/j.clet.2024.100759.
[31] S. Rajendran, G. Palani, V. Shanmugam, A. Kanagaraj, A. Veerasimman, U. Marimuthu, Comparative analysis of mechanical and erosion performance of cashew and sugarcane waste based biochar-reinforced polyester composites, Clean. Eng. Technol. *18* (2024) 100718, https://doi.org/10.1016/j.clet.2023.100718.
[32] Q. Zhang, D. Zhang, H. Xu, W. Lu, X. Ren, H. Cai, H. Lei, E. Huo, Y. Zhao, M. Qian, et al., Biochar filled high-density polyethylene composites with excellent properties: towards maximizing the utilization of agricultural wastes, Ind. Crops Prod. *146* (2020) 112185, https://doi.org/10.1016/j.indcrop.2020.112185.
[33] M.R. Snowdon, F. Wu, A.K. Mohanty, M. Misra, Comparative study of the extrinsic properties of poly(lactic acid)-based biocomposites filled with talc: versus sustainable biocarbon, RSC Adv. *9* (2019) 6752–6761, https://doi.org/10.1039/c9ra00034h.
[34] O. Das, N.K. Kim, A.L. Kalamkarov, A.K. Sarmah, D. Bhattacharyya, Biochar to the rescue: balancing the fire performance and mechanical properties of polypropylene composites, Polym. Degrad. Stab. *144* (2017) 485–496, https://doi.org/10.1016/j.polymdegradstab.2017.09.006.
[35] O. Das, N.K. Kim, A.K. Sarmah, D. Bhattacharyya, Development of waste based biochar/wool hybrid biocomposites: flammability characteristics and mechanical properties, J. Clean. Prod. *144* (2017) 79–89, https://doi.org/10.1016/j.jclepro.2016.12.155.
[36] F. Tomiak, K. Rathberger, A. Schöffel, D. Drummer, Expandable graphite for flame retardant pa6 applications, Polym. (Basel) *13* (2021), https://doi.org/10.3390/polym13162733.
[37] H. Qin, S. Zhang, C. Zhao, G. Hu, M. Yang, Flame retardant mechanism of polymer/clay nanocomposites based on polypropylene, Polym. (Guildf.) *46* (2005) 8386–8395, https://doi.org/10.1016/j.polymer.2005.07.019.
[38] A. Kausar, I. Rafique, B. Muhammad, Significance of carbon nanotube in flame retardant polymer/CNT composite: a review, Polym. Plast. Technol. Eng. *56* (2017) 470–487, https://doi.org/10.1080/03602559.2016.1233267.
[39] F.Y. Hshieh, Shielding effects of silica-ash layer on the combustion of silicones and their possible applications on the fire retardancy of organic polymers, Fire Mater. *22* (1998) 69–76, https://doi.org/10.1002/(sici)1099-1018(199803/04)22:2<69::aid-fam640>3.3.co;2-l.
[40] Q. Zhao, B. Zhang, H. Quan, R.C.M. Yam, R.K.K. Yuen, R.K.Y. Li, Flame retardancy of rice husk-filled high-density polyethylene ecocomposites, Compos. Sci. Technol. *69* (2009) 2675–2681, https://doi.org/10.1016/j.compscitech.2009.08.009.
[41] E.M. Ginting, Motlan, R.A. Sani, N. Bukit, B.F. Bukit, Utilization of eco-friendly rice husk ash waste as reinforcement in LDPE thermoplastics, Ecol. Eng. Environ. Technol. *24* (2023) 240–246, https://doi.org/10.12912/27197050/171867.
[42] M. Sain, S.H. Park, F. Suhara, S. Law, Flame retardant and mechanical properties of natural fibre-pp composites containing magnesium hydroxide, Polym. Degrad. Stab. *83* (2004) 363–367, https://doi.org/10.1016/S0141-3910(03)00280-5.
[43] A. Schirp, A. Barrio, Fire Retardancy of polypropylene composites reinforced with rice husks: from oxygen index measurements and cone calorimetry to large-scale single-burning-item tests, J. Appl. Polym. Sci. *135* (2018) 1–18, https://doi.org/10.1002/app.46654.
[44] Q. Zhang, J. Chen, X. Guo, H. Lei, R. Zou, E. Huo, X. Kong, W. Liu, M. Wang, Z. Ma, et al., Mussel-Inspired polydopamine-modified biochar microsphere for reinforcing polylactic acid composite films: emphasizing the achievement of excellent thermal and mechanical properties, Int. J. Biol. Macromol. *260* (2024) 129567, https://doi.org/10.1016/j.ijbiomac.2024.129567.
[45] Q. Zhang, R. Wang, W. Liu, Y. Yang, L. Huang, E. Huo, Z. Ma, New strategy for reinforcing polylactic acid composites: towards the insight into the effect of biochar microspheres, Int. J. Biol. Macromol. *245* (2023) 125487, https://doi.org/10.1016/j.ijbiomac.2023.125487.
[46] V.A. Yiga, M. Lubwama, P.W. Olupot, Pyrolysis, kinetics and thermodynamic analyses of rice husks/clay fiber-reinforced polylactic acid composites using thermogravimetric analysis, J. Therm. Anal. Calorim. *148* (2023) 3457–3477, https://doi.org/10.1007/s10973-022-11927-y.
[47] Joseph H. Flynn, L.A.W.A. Quick, Direct method for the determination of activation energy from thermogravimetric data, J. Polym. Sci. Part B Polym. Lett. *4* (1966) 323–328, https://doi.org/10.1002/pol.1966.110040504.
[48] J.H. Flynn, L.A. Wall, Initial kinetic parameters from thermogravimetric rate and conversion data, J. Polym. Sci. Part B Polym. Lett. *5* (1967) 191–196, https://doi.org/10.1002/pol.1967.110050211.
[49] A. Tagliaferro, M. Rovere, E. Padovano, M. Bartoli, M. Giorcelli, Introducing the novel mixed gaussian-lorentzian lineshape in the analysis of the raman signal of biochar, Nanomaterials *10* (2020) 1–19, https://doi.org/10.3390/nano10091748.
[50] Y. Katoh, M. Okamoto, Crystallization controlled by layered silicates in nylon 6-clay nano-composite, Polym. (Guildf.) *50* (2009) 4718–4726, https://doi.org/10.1016/j.polymer.2009.07.019.
[51] J.H. Flynn, L.A.A. Quick Wall, Direct method for the determination of activation energy from thermogravimetric data, J. Polym. Sci. Part B Polym. Lett. (*4*) (1966) 323–328, https://doi.org/10.1098/rstb.1988.0133.
[52] N. Vasanthan, D.R. Salem, FTIR spectroscopic characterization of structural changes in polyamide-6 fibers during annealing and drawing, J. Polym. Sci. Part B Polym. Phys. *39* (2001) 536–547, https://doi.org/10.1002/1099-0488(20010301)39:5<536::AID-POLB1027>3.0.CO;2-8.
[53] N. Vasanthan, D.R. Salem, Infrared spectroscopic characterization of oriented polyamide 66: band assignment and crystallinity measurement, J. Polym. Sci. Part B Polym. Phys. *38* (2000) 516–524, https://doi.org/10.1002/(SICI)1099-0488(20000215)38:4<516::AID-POLB3>3.0.CO;2-Y.
[54] E.O. Ogunsona, M. Misra, A.K. Mohanty, Impact of interfacial adhesion on the microstructure and property variations of biocarbons reinforced nylon 6 biocomposites, Compos. Part A Appl. Sci. Manuf. *98* (2017) 32–44, https://doi.org/10.1016/j.compositesa.2017.03.011.
[55] M.H. Morcali, B. Zeytuncu, O. Yucel, Platinum uptake from chloride solutions using biosorbents, Mater. Res. *16* (2013) 528–538, https://doi.org/10.1590/S1516-14392013005000006.
[56] F. Tuinstra, J.L. Koenig, Raman spectrum of graphite, J. Chem. Phys. *53* (1970) 1126–1130, https://doi.org/10.1063/1.1674108.
[57] D. Torsello, G. Ghigo, M. Giorcelli, M. Bartoli, M. Rovere, A. Tagliaferro, Tuning the microwave electromagnetic properties of biochar-based composites by annealing, Carbon Trends *4* (2021) 100062, https://doi.org/10.1016/j.cartre.2021.100062.
[58] N.S. Murthy, Metastable crystalline phases in nylon 6, Polym. Commun. (1991) *32*.

[59] Yanzhu Zhang, Yi Zhang, Siwei Liu, Aiping Huang, Zhenguo Chi, Jiarui Xu, J. E. Phase, Stability and Melting behavior of the a and c phases of nylon 6, J. Appl. Polym. Sci. *120* (2011) 1885–1891, https://doi.org/10.1002/app.33047.
[60] A. Mohanty, S. Vivekanandhan, A. Anstey, M. Misra, Sustainable composites from renewable biochar and engineering plastic, ICCM Int. Conf. Compos. Mater. (2015) 19–24. *2015-July*.
[61] O. Das, A.K. Sarmah, D. Bhattacharyya, A novel approach in organic waste utilization through biochar addition in wood/polypropylene composites, Waste Manag *38* (2015) 132–140, https://doi.org/10.1016/j.wasman.2015.01.015.
[62] G. De Bhowmick, A.K. Sarmah, R. Sen, Production and characterization of a value added biochar mix using seaweed, rice husk and pine sawdust: a parametric study, J. Clean. Prod. *200* (2018) 641–656, https://doi.org/10.1016/j.jclepro.2018.08.002.
[63] F.S.M. Sinfrônio, J.C.O. Santos, L.G. Pereira, A.G. Souza, M.M. Conceição, V. J. Fernandes, V.M. Fonseca, Kinetic of thermal degradation of low-density and high-density polyethylene by non-isothermal thermogravimetry, J. Therm. Anal. Calorim. *79* (2005) 393–399, https://doi.org/10.1007/s10973-005-0072-4.
[64] M. Gray, M.G. Johnson, M.I. Dragila, M. Kleber, Water uptake in biochars: the roles of porosity and hydrophobicity, Biomass-.-. Bioenergy *61* (2014) 196–205, https://doi.org/10.1016/j.biombioe.2013.12.010.
[65] D. Singh Karam, P. Nagabovanalli, K. Sundara Rajoo, C. Fauziah Ishak, A. Abdu, Z. Rosli, F. Melissa Muharam, D. Zulperi, An overview on the preparation of rice husk biochar, factors affecting its properties, and its agriculture application, J. Saudi Soc. Agric. Sci. *21* (2022) 149–159, https://doi.org/10.1016/j.jssas.2021.07.005.
[66] S. Zhu, Y. Guo, Y. Chen, S. Liu, Low water absorption, high-strength polyamide 6 composites blended with sustainable bamboo-based biochar, Nanomaterials *10* (2020) 1–15, https://doi.org/10.3390/nano10071367.
[67] L. Botta, R. Teresi, V. Titone, G. Salvaggio, F.P. La Mantia, F. Lopresti, Use of biochar as filler for biocomposite blown films: structure-processing-properties relationships, Polymers *13* (2021) 3953, https://doi.org/10.3390/polym13223953.
[68] M. Cappello, D. Rossi, S. Filippi, P. Cinelli, M. Seggiani, Wood residue-derived biochar as a low-cost, lubricating filler in poly(butylene succinate-Co-adipate) biocomposites, Materials *16* (2023) 570, https://doi.org/10.3390/ma16020570.
[69] Alper Kiziltas, Behzad Nazari, Douglas J. Gardner, D.W.B. polyamide 6-cellulose composites: effect of cellulose composition on melt rheology and crystallization behavior, Polym. Eng. Sci. *54* (2014) 739–746, https://doi.org/10.1002/pen.23603.
[70] Q. Zhang, K. Li, Y. Fang, Z. Guo, Y. Wei, K. Sheng, Conversion from bamboo waste derived biochar to cleaner composites: synergistic effects of aramid fiber and silica, J. Clean. Prod. *347* (2022) 131336, https://doi.org/10.1016/j.jclepro.2022.131336.
[71] E. Watt, M.A. Abdelwahab, A.K. Mohanty, M. Misra, Biocomposites from biobased polyamide 4,10 and waste corn cob based biocarbon, Compos. Part A Appl. Sci. Manuf. *145* (2021) 106340, https://doi.org/10.1016/j.compositesa.2021.106340.
[72] G. Strangis, D. Rossi, P. Cinelli, M. Seggiani, Seawater biodegradable poly(butylene succinate- co -adipate) - wheat bran biocomposites, Materials *16* (2023), https://doi.org/10.3390/ma16072593.
[73] S.C. Peterson, C.M. McMahan, Replacement of carbon black with coppiced biochar in guayule rubber composites improves tensile properties, J. Compos. Sci. *7* (2023) 1–12, https://doi.org/10.3390/jcs7120499.
[74] R. Arrigo, M. Bartoli, G. Malucelli, Poly(Lactic Acid)–biochar biocomposites: effect of processing and filler content on rheological, thermal, and mechanical properties, Polymers *12* (2020) 892, https://doi.org/10.3390/polym12040892.
[75] G.D. Biricik, H. Celebi, A.T. Seyhan, F. Ates, Thermal and mechanical properties of flax char/carbon fiber reinforced polyamide 66 hybrid composites, Polym. Compos. *43* (2022) 503–516, https://doi.org/10.1002/pc.26394.